Supporting Information

Mo_2C-derived Molybdenum Oxycarbides Afford Controllable Oxidation of Anilines to Azobenzenes and Azoxybenzenes

Zhe Wang,[a] Yimei Chen,[a] Zhouyang Long,*[,b] Yunfei Wang,[a] Mingming Fan,[a] Pingbo Zhang,[a] and Yan Leng*[,a]

[a] Key Laboratory of Synthetic and Biological Colloids, Ministry of Education, School of Chemical and Material Engineering, Jiangnan University, Wuxi 214122 (China)

E-mail: yanleng@jiangnan.edu.cn

[b] Jiangsu Key Laboratory of Green Synthetic Chemistry for Functional Materials, School of Chemistry & Materials Science, Jiangsu Normal University, Xuzhou 221116 (China)

E-mail: longzhouyangfat@163.com

Table of Content

Experimental Section

Characterizations

The crystallinity and phase of the samples were characterized using XRD. The XRD spectra of the catalysts were obtained using a Bruker AXS D8 X-advanced powder diffractometer with tube current and voltage settings of 40 mA and 40 kV, respectively, equipped with a solid-state detector and Cu Kα radiation, with a scanning range of 5-90° and a scanning rate of 5°/min. XPS was performed on the surface chemical state of the samples at 12 kV, 12 mA Al Ka X-ray source (1486.6 eV) under the surface chemical state of the samples was tested under the conditions of a 12 kV, 12 mA Al Ka X-ray source (1486.6 eV). The binding energy was corrected using the C 1s peak (284.6 eV) as a reference to minimize the charge effect of the sample. The TEM was done on a FEI Talos F200X G2 transmission electron microscope. The samples were dissolved in anhydrous ethanol and the mixture was sonicated for 5 min. Energy–dispersive X–ray spectroscopy (EDS) mapping was also combined for elemental analysis. Infrared spectra were performed using an FT-IR instrument with a Nicolet iS50, and the wavelength range was chosen to be 4000-500 cm^{-1}. The catalyst porous structure parameters were determined by Brunauer-Emmett-Teller (BET) method by N_2 adsorption-desorption isotherms using a Micromeritics ASAP 2460 at 77K. The pore volume and pore size of the samples were calculated by Barrett-Joyner-Halenda (BJH) method.

DFT calculations

Slab models of Mo_2C surface (002-Mo and 002-C, 3-layered, 3 × 5 supercell) were built according to Ref.1. In order to avoid interactions between periodic images, a vacuum distance of 20 Å was imposed between different layers. Aiming to investigate whether molecular oxygen (O_2) would decompose on the Mo_2C surface, the periodic Ab initio molecular dynamics (AIMD) simulations were carried out with the CP2K package version-2022.1 using Gaussian Plane Wave (GPW) method implemented in the QUICKSTEP module.[2] Norm-conserving Goedecker-Teter-Hutter (GTH) pseudopotentials for core electrons were used[3-5] and the valence electron wavefunction was expanded in a Double-zeta valence polarized (DZVP) sets.[6] Plane wave and relative cut-offs were set to 300 and 40 Ry, respectively. The generalized gradient approximation exchange-correlation energy was calculated using the Perdew-Burke-Ernzerhof (PBE)[7] functional with the DFT-D3

damped dispersion corrections of Grimme *et al*.[8] The AIMD simulations were performed in the canonical ensemble (NVT) at 298.15 K. The temperature of the AIMD-simulated system was controlled using a CSVR thermostat.[9] Production runs were 2000 fs long with a time step of 0.5 fs. All of the AIMD trajectory movies can be found in the Supporting Information.

The adsorption energy values were calculated using CP2K,[10] using Gaussian Plane Wave (GPW) method implemented in the QUICKSTEP module. Perdew-Burke-Ernzerhof (PBE) exchange-correlation (XC) functional with Grimme-D3 dispersion correction method was employed. Both the double-zeta valence polarized (DZVP) sets and Goedecker-Teter-Hutter (GTH) pseudopotentials were adopted. Plane wave and relative cut-offs were set to 400 and 55 Ry, respectively. The inner and outer SCF convergence criteria were set to 2.0×10^{-6} Ha. In order to avoid interactions between periodic images, a vacuum distance of 20 Å was imposed between different layers. The geometrical optimizations were implemented at the *Γ* point for all surface structures. The bottom two layers of atoms were frozen while the top two were allowed to relax. Root mean square and maximum force convergence were set to 3.0×10^{-4} and 4.5×10^{-4} Ha·Å^{-1}, respectively.

The adsorption energies were calculated according to equation (1),

$$E_{ads} = E_{(slab + adsorbate)} - E_{(slab)} - E_{(adsorbate)} \quad (1)$$

where $E_{(slab + adsorbate)}$, $E_{(slab)}$, and $E_{(adsorbate)}$ are the calculated electronic energy of species adsorbed on the surface, the bare surface, and the gas-phase molecule, respectively.[3-5, 11, 12]

DFT calculations for cluster models were performed using Gaussian 09 program (version D.01).[13-15] Geometry optimization was conducted at the B3LYP/def2-SVP level of theory, which were dispersion corrected by D3BJ; the single point calculations for the optimized geometries were performed to obtain accurate energies at the M062x/def2-TZVP level of theory, which were dispersion corrected by D3.[16-19] Vibrational frequency analysis was carried out to identify the nature of each stationary points as a minimum or a transition state, and to acquire the Gibbs free energy correction. The solvent effects were considered with one solvent molecule, H_2O or AcOH, combined with corresponding SMD solvation models. The Gibbs free energies were included in the Gibbs energy correction of unscaled vibrational analysis at the B3LYP/def2-SVP (D3BJ) level of theory.

Classical molecular dynamics simulations

The mixtures of cyclohexane/H_2O_2/H_2O (5:1:4) and AcOH/H_2O_2/H_2O (9:1:4) were simulated through molecular dynamics (MD). The MD simulations were conducted using the GROMACS package (version: 2020.6).[20, 21] The amber99sb force field were used to parametrize all atoms, such as the bond parameters, angle parameters and the dihedral angles, and so on. The RESP charges of molecules were obtained by using Gaussian 09 and Multiwfn at the B3LYP/6-311+g (d,p) level. TIP3P was used for the model of water molecule. The steepest descent method was applied to minimize the initial energy for each system with a force tolerance of 1 kJ/(mol^{-1} nm^{-1}) and a maximum step size of 0.002 ps before MD calculations. In all the three directions, periodic boundary conditions were imposed. Leapfrog algorithm was used to integrate the Newtonian equation of motion (time step=2.0 fs, bonds to hydrogen atoms were maintained with the LINCS algorithm). The MD simulation was processed in an NVT ensemble and the simulation time is 20 ns at 353.15 K. The Particle-Mesh-Ewald (PME) with a fourth-order interpolation was used to evaluate the electrostatic interactions and the grid spacing is 1.0 Å, whereas a cutoff of 1.0 Å was employed to calculate the short-range van der Waals interactions. The simulation results were visualized and analyzed with VMD.[4]

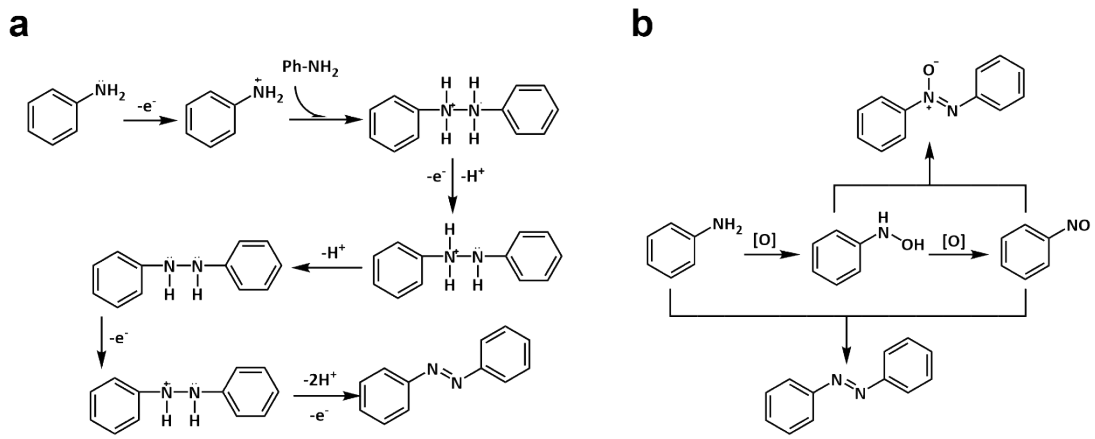

Scheme S1. The reaction pathways of aniline oxidation. (a) aniline radical mechanism; (b) the nitrosobenzene intermediate mechanism.

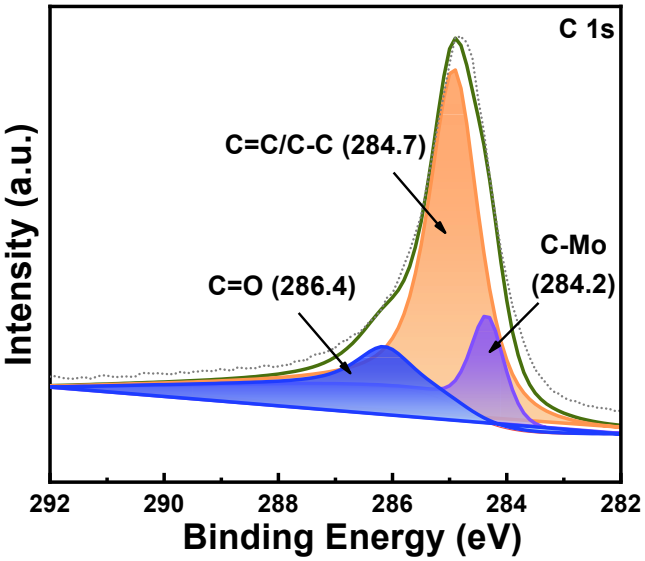

Fig. S1 C 1s XPS spectra of Mo_2C@C.

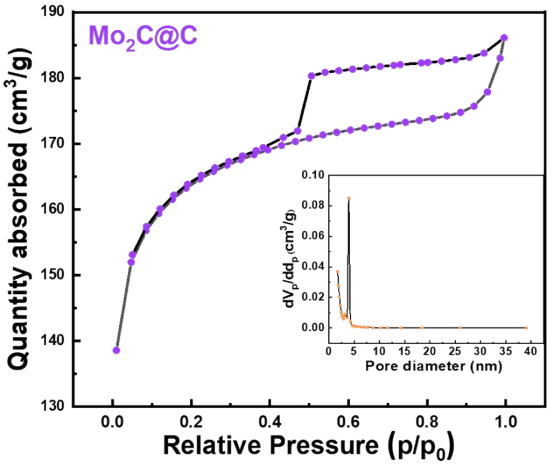

Fig. S2 N_2 adsorption-desorption isotherms and pore-size distribution of Mo_2C@C.

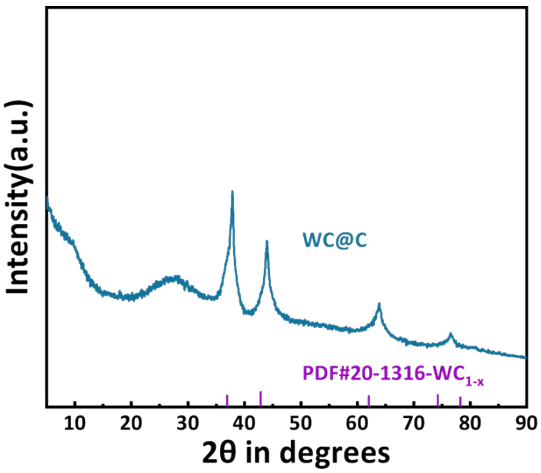

Fig. S3 XRD pattern of WC@C.

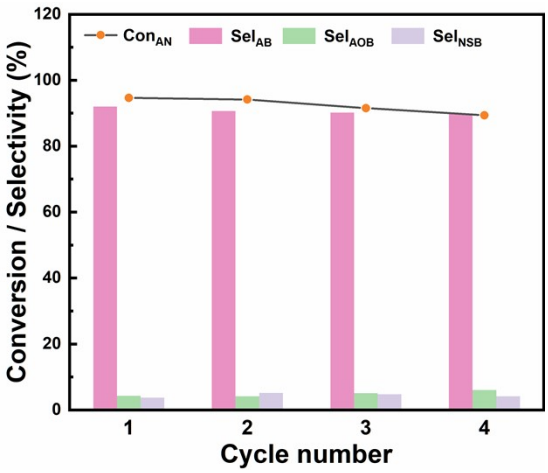

Fig. S4 Reusability of Mo_2C@C-catalyzed oxidative coupling of anilines.

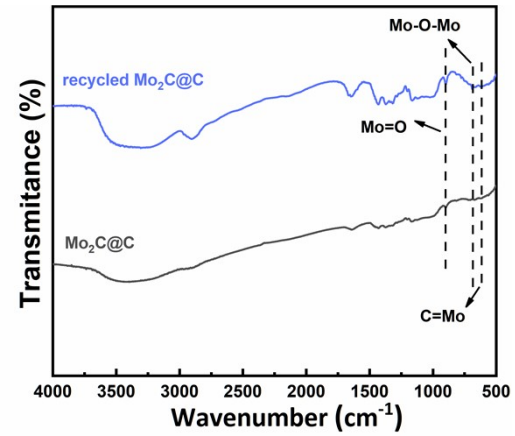

Fig. S5 Comparison of FTIR spectra of recycled and fresh catalysts.

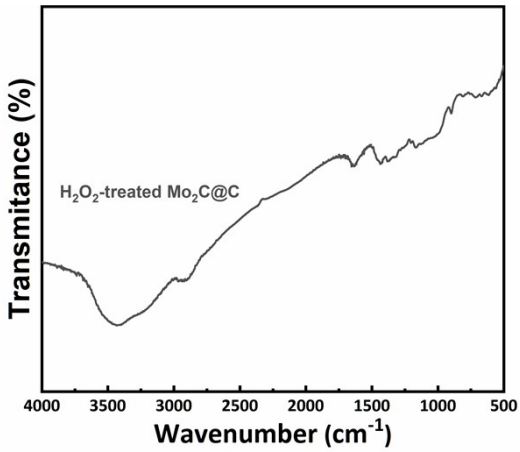

Fig. S6 FTIR spectra of H_2O_2-treated Mo_2C@C.

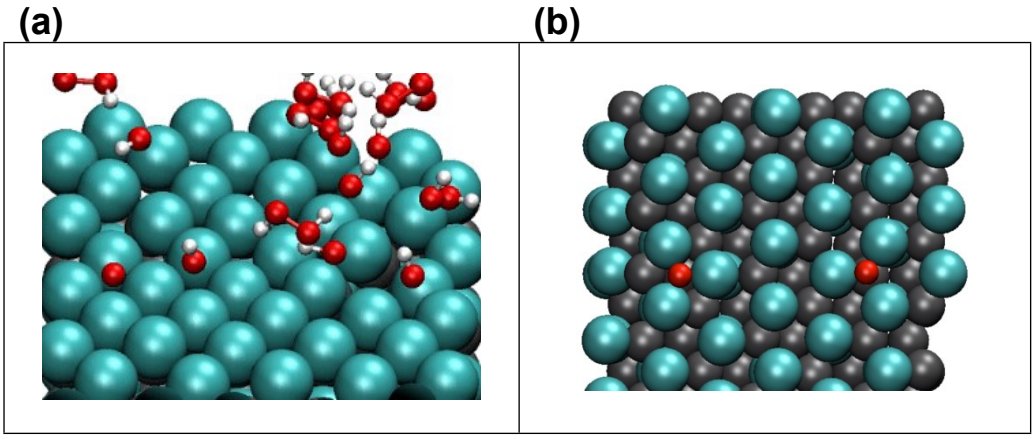

Fig. S7 AIMD simulations results of (a) H_2O_2 and (b) O_2 decomposition on the Mo_2C@C surface. The complete decomposition process can be found in the attached video.

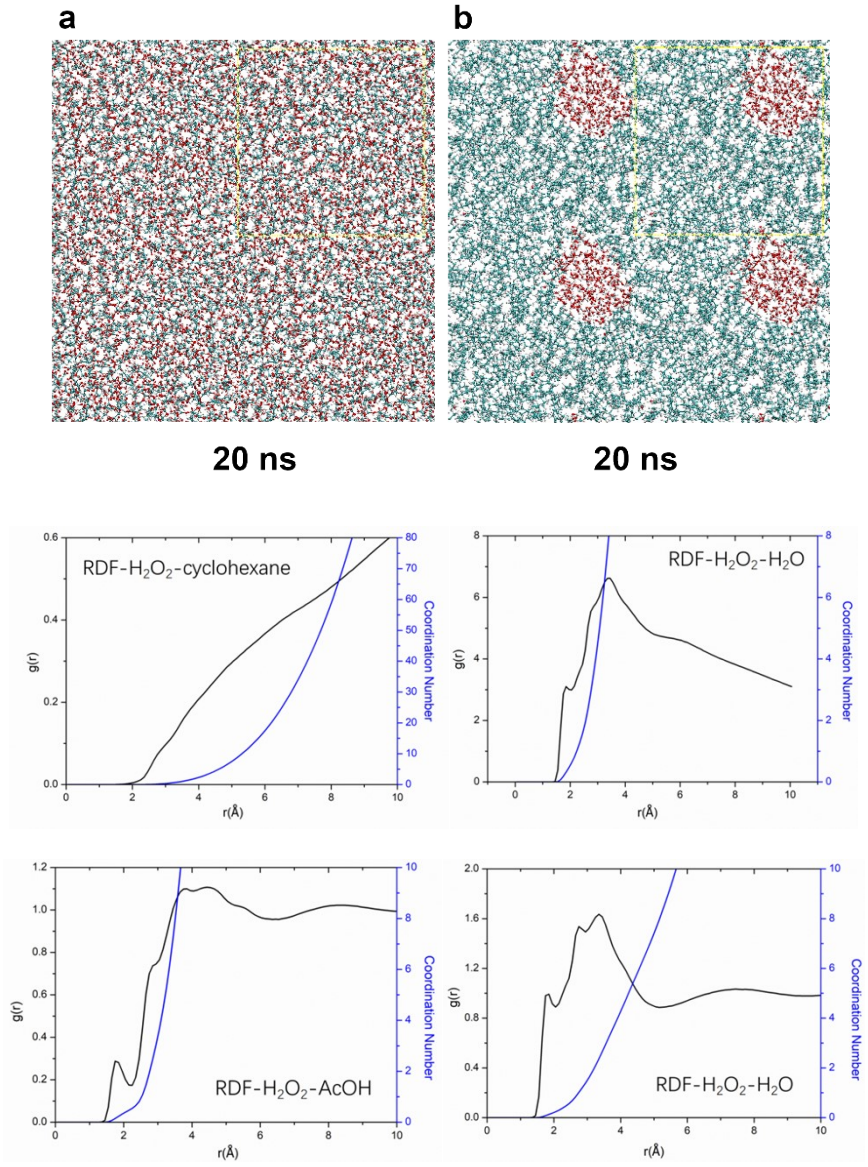

Fig. S8 Molecular dynamics simulations of aqueous solutions of H_2O_2 in (a) acetic acid and (b) cyclohexane solvents, and the corresponding radial distribution function (RDF). The green parts represent acetic acid and cyclohexane, respectively, and the red parts represent H_2O_2 and H_2O.

Fig. S9 Contact angle test of catalyst MoC_xO_y.

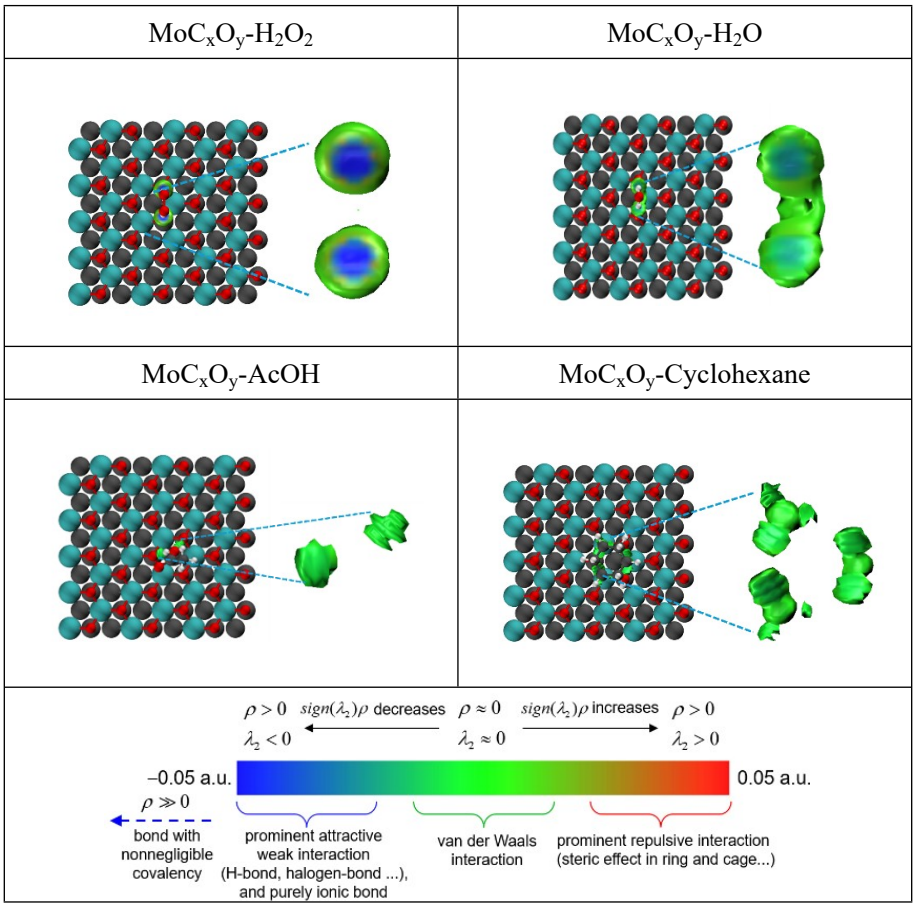

Fig. S10 IGMH analysis for different solvent molecules on the surface of MoC_xO_y.

a. MoC_xO_y-H_2O (Cyclohexane as the solvent) system

IM1	TS_{1-2}	IM2	TS_{2-3}
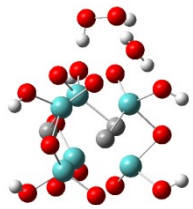	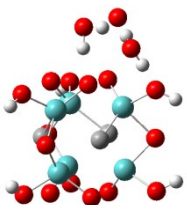	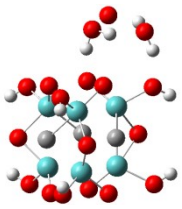	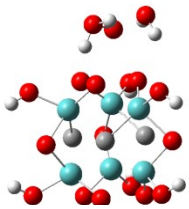
IM3	TS_{3-4}	IM4	IM5
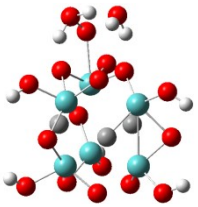	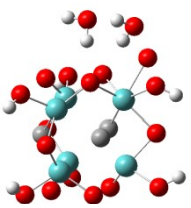	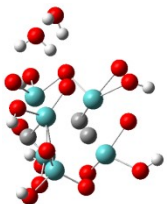	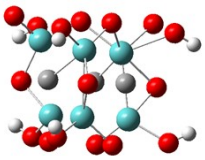
IM6	TS_{6-7}	IM7	TS_{7-8}
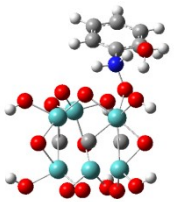	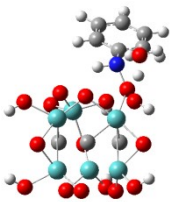	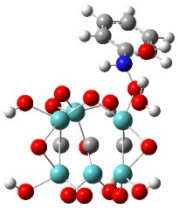	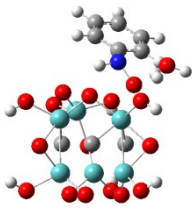
IM8			
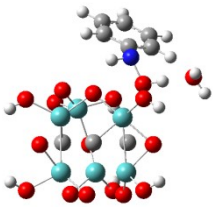			

Fig. S11 The initial structure, transition state, and the final structure of aniline oxidation to Ph-NHOH on Mo_2C with H_2O_2 in H_2O/Cyclohexane solvent.

b. MoC_xO_y-AcOH (AcOH as the solvent) system

IM1	TS_{1-2}	IM2	IM3
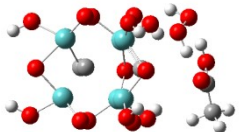	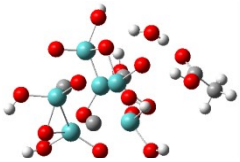	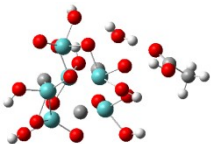	
IM4	TS_{4-5}	IM5	
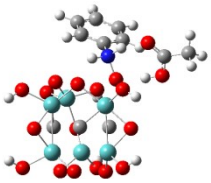	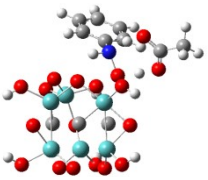	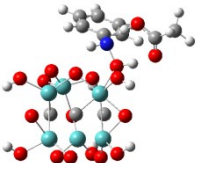	

Fig. S12 The initial structure, transition state, and the final structure of aniline oxidation to Ph-NHOH on Mo_2C with H_2O_2 in AcOH solvent.

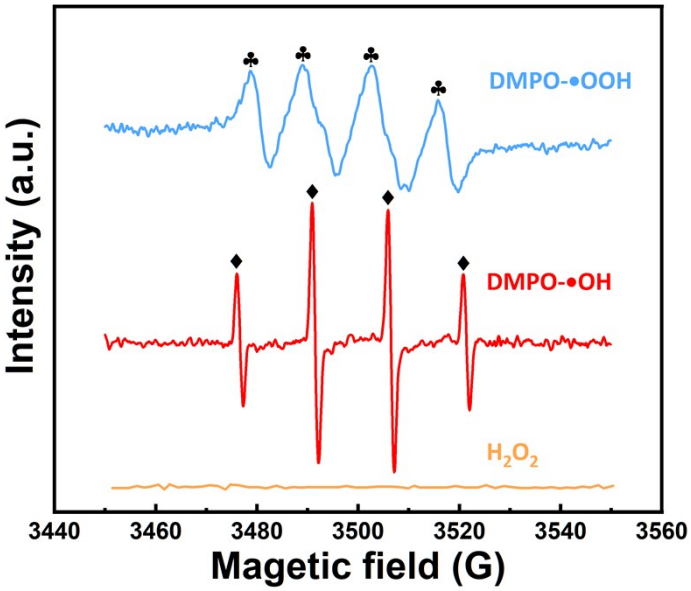

Fig. S13 EPR spectra of the Mo_2C-H_2O_2 system.

Table S1. Oxidative coupling of aniline reported in previous literatures.

Catalyst	Solvent	Time (h)	T (°C)	Oxidant	Con (%)	Sel (%)			Ref
						AB	AOB	NSB	
CuBr-pyridine	Toluene	20	60	Air		97 yield of AB			22
Au_1Pd_3@C-KOH	DMSO	12	60	O_2	98	99	-	-	23
Ag/C-KOH	DMSO	24	60	Air		97 yield of AB			24
Au/CeO_2	Toluene	10	100	O_2	100	93	-	-	25
RuO_2/Cu_2O	CH_3CN	16	85	Air		94 yield of AB			26
$Ag_{0.6}Ni_{0.4}$-KOH	DMSO	24	60	Air		94 yield of AB			27
MnO_x	PhCl	24	160	O_2	95	99	-	-	28
NT-MnOOH	Toluene	12	60	O_2	99	AB > 99.9			29
Ag/Fe_2O_3	CH_3CN	8	50	H_2O_2	92	-	94	-	30
Ag/WO_3	CH_3CN	24	25	H_2O_2	99	-	99	-	31
TBA_6-Nb	Ethanol	5	30	H_2O_2	99	-	97	-	32
Nb_2O_5/FeOOH	Propanol	24	25	H_2O_2	99	16	80	3	33
$CuCr_2O_4$	1,4-dioxane	10	70	H_2O_2	78	-	92	-	34
$[N(C_4H_9)_4]_2[Mo_6O_{19}]$-$Na_2S_2O_3$	MeOH	24	60	H_2O_2		95 yield of AB			35
	MTBE	36	50	H_2O_2		90 yield of AOB			
	Methanol	2	rt	H_2O_2	98	0	98	2	
$Zr(OH)_4$	AcOH	24	40	TBHP	96	94	3	1	36
	Mesitylene	4	rt	H_2O_2	96	0	12	88	
Mo_2C@C	Acetic acid	6	80	H_2O_2	> 99	99	1	-	This work
Mo_2C@C	Cyclohexane	6	80	H_2O_2	> 99	5	95	-	

Table S2. Investigations into the reaction mechanism involving the acetic acid and cyclohexane system.

Entry	Substrate	Catalyst	H_2O_2 equivalent	Solvent	T [°C]	Time [h]	Con	Sel of AB	Sel of AOB	Sel of NSB
1	Ph-NH_2+ BHT[a]	Mo_2C@C	2	acetic acid	80	6	94	90	6	4
2	Ph-NH_2+ BHT[a]	Mo_2C@C	2	cyclohexane	80	6	61	1	72	27
3	Ph-NHOH[b]	Mo_2C@C	2	acetic acid	rt	1	100	1	98	1
4	Ph-NHOH[b]	Mo_2C@C	0.5	acetic acid	rt	1	100	1	97	2
5	Ph-NHOH[b]	Mo_2C@C	2	cyclohexane	rt	1	100	1	94	5
6	Ph-NHOH+ Ph-NO[c]	-	-	acetic acid	rt	6	100	1	99	0
7	Ph-NHOH+ Ph-NO[c]	-	-	cyclohexane	rt	1	98	0	100	0
8	$PhNH_2$+Ph-NO[d]	-	-	acetic acid	rt	6	100	98	2	0
9	Ph-NH_2+Ph-NO[d]	-	-	cyclohexane	80	6	-	-	-	-

[a] Reaction conditions: aniline (2 mmol), BHT (2.4 mmol), catalyst (20 mg), solvent (2 mL), oxidant (H_2O_2, 30 wt%). [b] Reaction conditions: Ph-NHOH (2 mmol), catalyst (20 mg), solvent (2 mL), oxidant (H_2O_2, 30 wt%). [c] Reaction conditions: Ph-NHOH (1 mmol), Ph-NO (1 mmol), solvent (2 mL), oxidant (H_2O_2, 30 wt%). [d] Reaction conditions: Ph-NH_2 (1 mmol), Ph-NO (1 mmol), solvent (2 mL), oxidant (H_2O_2, 30 wt%). Conversion and selectivity were determined by GC analysis.

References

1. X. Liu, C. Kunkel, P. Ramírez de la Piscina, N. Homs, F. Viñes and F. Illas, *ACS Catal.*, 2017, **7**, 4323-4335.
2. T. D. Kuhne, M. Iannuzzi, M. Del Ben, V. V. Rybkin, P. Seewald, F. Stein, T. Laino, R. Z. Khaliullin, O. Schutt, F. Schiffmann, D. Golze, J. Wilhelm, S. Chulkov, M. H. Bani-Hashemian, V. Weber, U. Borstnik, M. Taillefumier, A. S. Jakobovits, A. Lazzaro, H. Pabst, T. Muller, R. Schade, M. Guidon, S. Andermatt, N. Holmberg, G. K. Schenter, A. Hehn, A. Bussy, F. Belleflamme, G. Tabacchi, A. Gloss, M. Lass, I. Bethune, C. J. Mundy, C. Plessl, M. Watkins, J. VandeVondele, M. Krack and J. Hutter, *J. Chem. Phys.*, 2020, **152**, 194103.
3. T. Lu and F. Chen, *J. Comput. Chem.*, 2012, **33**, 580-592.
4. W. Humphrey, A. Dalke and K. Schulten, *J. Mol. Graph.*, 1996, **14**, 33-38, 27-38.
5. J. Zhang and T. Lu, *Phys. Chem. Chem. Phys.*, 2021, **23**, 20323-20328.
6. J. VandeVondele, M. Krack, F. Mohamed, M. Parrinello, T. Chassaing and J. Hutter, *Comput. Phys. Commun.*, 2005, **167**, 103-128.
7. S. Goedecker, M. Teter and J. Hutter, *Phys. Rev. B*, 1996, **54**, 1703-1710.
8. C. Hartwigsen, S. Goedecker and J. Hutter, *Phys. Rev. B*, 1998, **58**, 3641-3662.
9. G. Bussi, D. Donadio and M. Parrinello, *J. Chem. Phys.*, 2007, **126**, 014101.
10. Y. Wang, J. Guo, S. Li, Y. Sun, Z. Long, L. Shen and C. Lai, *ACS Appl. Mater. Interfaces,* 2023, **15**, 54510-54519.
11. Y. Li, Z. Wang, H. Gu, H. Jia, Z. Long and X. Yan, *ACS Nano*, 2024, **18**, 8863-8875.
12. T. Lu and Q. Chen, *J. Comput. Chem.*, 2022, **43**, 539-555.
13. W. J. Hehre, R. Ditchfield and J. A. Pople, *J. Chem. Phys.*, 1972, **56**, 2257-2261.
14. R. Krishnan, J. S. Binkley, R. Seeger and J. A. Pople, *J. Chem. Phys.*, 1980, **72**, 650-654.
15. M. Caricato, G. Scalmani, G. W. Trucks and M. J. Frisch, *J. Phys. Chem. Lett.*, 2010, **1**, 2369-2373.
16. F. Weigend and R. Ahlrichs, *Phys. Chem. Chem. Phys.*, 2005, **7**, 3297-3305.
17. S. Grimme, J. Antony, S. Ehrlich and H. Krieg, *J. Chem. Phys.*, 2010, **132**, 154104.
18. S. Grimme, S. Ehrlich and L. Goerigk, *J. Comput. Chem.*, 2011, **32**, 1456-1465.
19. Y. Li, J. Carroll, B. Simpkins, D. Ravindranathan, C. M. Boyd and S. Huo, *Organometallics*, 2015, **34**, 3303-3313.
20. H. J. C. Berendsen, D. van der Spoel and R. van Drunen, *Comput. Phys. Commun.*, 1995, **91**, 43-56.
21. D. Van Der Spoel, E. Lindahl, B. Hess, G. Groenhof, A. E. Mark and H. J. Berendsen, *J. Comput. Chem.*, 2005, **26**, 1701-1718.
22. C. Zhang and N. Jiao, *Angew. Chem., Int. Ed.,* 2010, **49**, 6174-6177.
23. F. Fu, S. He, S. Yang, C. Wang, X. Zhang, P. Li, H. Sheng and M. Zhu, *Sci. China Chem.*, 2015, **58**, 1532-1536.
24. S. Cai, H. Rong, X. Yu, X. Liu, D. Wang, W. He and Y. Li, *ACS Catal.*, 2013, **3**, 478-486.
25. Y. Pérez, C. Aprile, A. Corma and H. Garcia, *Catal. Lett.*, 2009, **134**, 204-209.
26. A. Saha, S. Payra, B. Selvaratnam, S. Bhattacharya, S. Pal, R. T. Koodali and S. Banerjee, *ACS Sustainable Chem. Eng.,* 2018, **6**, 11345-11352.
27. M. Kumar, K. Soni, G. D. Yadav, S. Singh and S. Deka, *Appl. Catal., A,* 2016, **525**, 50-58.
28. M. Wang, J. Ma, M. Yu, Z. Zhang and F. Wang, *Catal. Sci. Technol.,* 2016, **6**, 1940-1945.
29. Y. Zou, M. Zhang, F. Cao, J. Li, S. Zhang and Y. Qu, *J. Mater. Chem. A,* 2021, **9**, 19692-19697.
30. B. Paul, S. K. Sharma, S. Adak, R. Khatun, G. Singh, D. Das, V. Joshi, S. Bhandari, S. S. Dhar and R. Bal,

New J. Chem., 2019, **43**, 8911-8918.

31. S. Ghosh, S. S. Acharyya, T. Sasaki and R. Bal, *Green Chem.,* 2015, **17**, 1867-1876.
32. B. Ding, B. Xu, Z. Ding, T. Zhang, Y. Wang, H. Qiu, J. He, P. An, Y. Yao and Z. Hou, *Catal. Sci. Technol.,* 2022, **12**, 5360-5371.
33. A. L. D. Lima, D. C. Batalha, H. V. Fajardo, J. L. Rodrigues, M. C. Pereira and A. C. Silva, *Catal. Today,* 2020, **344**, 118-123.
34. S. S. Acharyya, S. Ghosh and R. Bal, *ACS Sustainable Chem. Eng.,* 2014, **2**, 584-589.
35. S. Han, Y. Cheng, S. Liu, C. Tao, A. Wang, W. Wei, H. Yu and Y. Wei, *Angew. Chem., Int. Ed.* 2021, **60**, 6382-6385.
36. J. Qin, Y. Long, F. Sun, P. P. Zhou, W. D. Wang, N. Luo and J. Ma, *Angew. Chem., Int. Ed.* 2022, **61**, e202112907.